Korean J. Chem. Eng., 36(10), 1746-1751 (2019)
DOI: 10.1007/s11814-019-0361-4

pISSN: 0256-1115
eISSN: 1975-7220

Photothermal performance of plasmonic patch with gold nanoparticles embedded on polymer matrix

Jaehwan Hong*, Dae Kun Hwang,***,****, Chulhwan Park*,†, and Younghun Kim*,†**

*Department of Chemical Engineering, Kwangwoon University, 20 Kwangwoon-ro, Nowon-gu, Seoul 01897, Korea
**Department of Chemical Engineering, Ryerson University, 350 Victoria St, Toronto, Ontario M5B 2N2, Canada
***Keenan Research Centre for Biomedical Science, St. Michael's Hospital, Toronto, Canada
****Institute for Biomedical Engineering, Science and Technology (iBEST) - a partnership between Ryerson University and St. Michael's Hospital, Toronto, Canada
(*Received 6 June 2019 • accepted 9 August 2019*)

Abstract−Under light irradiation, gold nanoparticles (AuNPs) reveal the surface plasmon feature, i.e., the occurrence of the collective excitation of the free electrons of NPs. Plasmon relaxation, as well as excitation, induced by light absorption, could be used to increase the local temperature via conversion of light to heat. This photothermal effect can be enhanced by control of the morphology and structure of NPs in the near-infrared (NIR) region. Recently, the use of an NP-composited polymer as a heating patch with a good photothermal performance was suggested for biomedical applications. Herein, AuNPs embedded on polydimethylsiloxane (PDMS) films (Au-PDMS) were successfully prepared with an in-situ synthesis method without a reducing agent. Their photothermal performance was measured with an IR camera under 808 nm NIR irradiation, and a mechanical stretching test for the Au-PDMS films was conducted to investigate the effect of the AuNPs' density on the photothermal performance. The surface temperature of the films, which reached 120 °C within 1 min, is also adjustable with mechanical stretching (strain change). This is due to the decrease of the AuNPs density with widening interparticle distance between them.

Keywords: Photothermal, Gold Nanoparticle, Surface Plasmon, Near-infrared, PDMS, Plasmonic Patch

INTRODUCTION

Metallic nanoparticles (NPs), such as gold or silver (AuNPs or AgNPs), present the surface plasmon resonance (SPR) feature in the visible to near-infrared (NIR) region of the spectrum [1]. Collective excitation occurs through the interaction of light with the free electrons of the NPs to reveal the SPR band [2]. Under plasmon excitation, NPs enhance the hole transfer (oxidation) or electron transfer (reduction), and thus they can act as an electron donor or acceptor in photocatalysts, solar cells, and electrochemical sensors [3-5]. Light absorption-induced plasmon relaxation, which simultaneously appears with plasmon excitation, has been considered as a side effect that should be minimized [6]. However, localized photothermal heating (thermo-plasmonic) via the light-to-heat conversion can be utilized in biomedical and photothermal applications, therapy [7,8], catalytic reactions [9], and imaging [10]. For example, in the case of an AuNP-TiO_2 photocatalyst, UV/visible light-driven 'hot' electrons on TiO_2 and the holes on AuNPs are used to reduce and oxidize target molecules, respectively, while NIR irradiation induces plasmonic-mediated heating effects [1]. In addition, the NIR laser-induced photothermal effect is useful for biomedical applications because NIR provides a deeper radiation penetration through biological soft tissues [8].

To enhance the photothermal properties and heat-conversion efficiency of plasmonic NPs, their structures (size, shape, and morphology) were modified. This structural modification induces the SPR coupling effect between neighboring NPs [11] or a significant redshift of the SPR band into the NIR region [12]. A metallic shell-dielectric core, such as silica beads coated with gold nanoshells, can give rise to an SPR band in the NIR region by changing the thickness of the gold nanoshell [13]. In case of single NPs suspended in solution, they can form aggregates or coagulators in a biological medium, which may indicate unexpected temperature changes with NIR irradiation.

Recently, AuNP-doped polymer matrices with photothermal characteristics, referred to as plasmonic patches, have attracted great interest for the preparation of optical film, antimicrobial coating, and artificial skin [14-16], due to their transparency, flexibility, and good thermal stability [17]. Among many, polydimethylsiloxane (PDMS) polymer has been widely used for fabricating plasmonic patches because of its popularity in biomedical applications.

However, controlling the photothermal properties of Au-PDMS films is challenging. One alternative pathway to control the local heating of the patches is to regulate the mechanical stretching of the films, because plasmonic NPs reveal a highly distance-dependent enhancement of photothermal heating as well as the SPR feature. Thus, the photothermal properties of Au-PDMS films can be readily adjustable through their mechanical stretching that alternates AuNPs' spacing in the PDMS matrix. Since this plasmonic patch exhibits a high optical absorption and thermal response with the

†To whom correspondence should be addressed.
E-mail: korea1@kw.ac.kr, chpark@kw.ac.kr

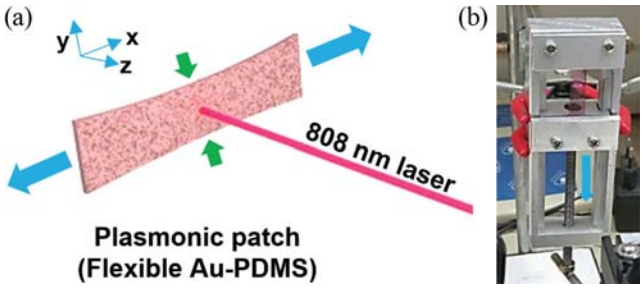

Fig. 1. (a) Schematic of stretching test of plasmonic patch (flexible Au-PDMS film), and (b) homemade clamps.

thermo-control ability via the simple mechanical streching, it has potential use in the biomedical field, such as for skin regeneration bandages for wounded or burn patients. When a plasmonic patch attached on human skin is exposed to visible or NIR light, the surface temperature of the patch may increase with changes to its photothermal properties. Therefore, the change in the photothermal properties, via mechanical stretching of the plasmonic patch, should be examined under NIR irradiation.

We prepared AuNP-embedded PDMS films (Au-PDMS) and analyzed their photothermal properties with mechanical stretching to adjust the interparticle distance of the AuNPs in the PDMS matrix. Upon stretching the Au-PDMS film in the *x*-axis direction (Fig. 1(a)), the AuNPs in the PDMS move further apart in the stretching direction, and closer together in the *y*-axis direction perpendicular to it [18]. Two competitive distance changes between neighboring AuNPs might lead to a change in the photothermal properties of Au-PDMS. For the in-situ preparation of the Au-PDMS films without an additional reducing agent, the residual curing agent in the PDMS elastomer itself is used to reduce the gold precursor ($HAuCl_4$) [19,20]. The AuNPs embedded in the PDMS matrix were found as ca. 24 nm and the final products showed free-standing films in a red-brown color, which varied with the concentration (0.011 to 0.056 wt%) of AuNPs in PDMS. The temperature changes of the Au-PDMS films were measured with mechanical strain under 808 nm NIR-laser irradiation (2 W/cm^2).

EXPERIMENTAL

1. Preparation of Au-PDMS Plasmonic Patch

Sylgard 184, including a PDMS elastomer (184A) and curing agent (184B) (Sigma-Aldrich), was used to prepare the polymer matrix, and $HAuCl_4$ (Kojima) was used as the precursor of the AuNPs. The Au-PDMS films with different concentrations of AuNPs in the PDMS were prepared by the following procedure. The uncured PDMS mixture was prepared by thorough mixing of the 184A and 184B agents in a 10 : 1 weight ratio. Without a reducing agent it is not easy to control the size of AuNPs in situ synthesis. Therefore, herein, we focused on the effect of AuNPs concentration and Au-PDMS strain as major parameters rather than the size of AuNPs. Different volumes of 25 mM $HAuCl_4$ solution, based on the ethyl alcohol, were mixed with the uncured PDMS mixture, yielding concentrations of AuNPs from 0.011 to 0.056 wt%. After vigorous mixing for 5 min, the resulting mixture was poured onto a petri dish and cured at 90 °C for 12 h in a vacuum-drying oven. The cured Au-PDMS films were peeled off the petri dish and cut into pieces of 20 mm×10 mm×1.3 mm. The Au-PDMS films were washed with anhydrous ethyl alcohol and dried rapidly with nitrogen gas.

2. Photothermal Performance

The photothermal performance was evaluated using an 808 nm NIR laser (2 W/cm^2). The distance between the Au-PDMS films and laser source was fixed at 15 cm. The temperature profile of the Au-PDMS films was recorded with an IR camera (Seek Thermal XR) for 5 min of heating by NIR laser and 2 min of cooling with the laser turned off. Mechanical stretching in the *x*-direction of the Au-PDMS films was carried out using homemade clamps to control the movement (Fig. 1(b)). The strain percentages in the parallel direction (length change, *x*-axis) with stretching and in the perpendicular direction (width change, *y*-axis) with shrinking were calculated with a Vernier caliper.

3. Characterization

The size of the AuNPs in the Au-PDMS films was measured by transmission electron microscopy (TEM, JEM-2010, Jeol), after dissolution of PDMS film with toluene. The UV-vis spectra of the Au-PDMS films were obtained by a spectrophotometer (UV-1800, Shimazdu).

RESULTS AND DISCUSSION

Herein, the AuNPs used for the preparation of a plasmonic patch are desirable and effective for biomedical applications due to their

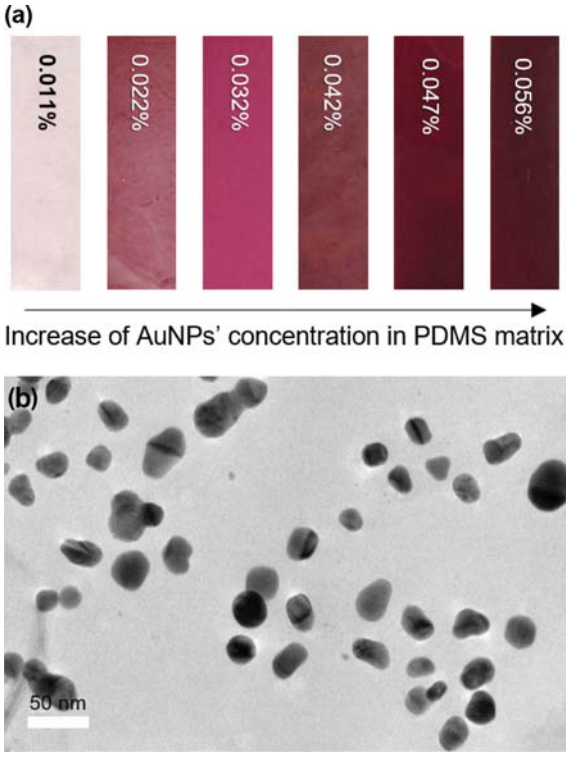

Fig. 2. (a) Color change of Au-PDMS films with increasing AuNP concentration in PDMS matrix, and (b) TEM image of AuNPs in Au-PDMS, which was obtained from toluene etching of Au-PDMS.

biocompatibility and tunable resonance feature with high absorption in the NIR region [21]. In addition, PDMS has outstanding elasticity, good thermal and oxidative stability, and an inert surface, promoting antifouling [17]; thus the Au-PDMS films may be acceptable as a potential scar bandage with the photothermal function.

The as-made Au-PDMS films are red-brown color depending on the concentration of AuNPs in the Au-PDMS, as shown in Fig. 2(a). Pure PDMS film is transparent, whereas the AuNP-embedded PDMS is red-brown, the characteristic color of AuNPs dispersed in solution. Thus, the transparency of Au-PDMS decreased with the AuNPs' content. To confirm AuNP formation in the PDMS matrix, aAu-PDMS film was dissolved with toluene. As shown in the TEM image (Fig. 2(b)), AuNPs with an average size of 24.1± 7.8 nm were obtained from the dissolved solution of the Au-PDMS film, which confirms that AuNPs are successfully embedded in the PDMS matrix. Several fabrication methods of Au-PDMS films have been reported, such as the incorporation of AuNPs into a PDMS matrix with a blending solvent [22], the immobilization of AuNPs on the surface of pre-treated PDMS [23], and the reduction of Au salts dispersed in uncured PDMS [20,24]. The previous two methods require premade AuNPs, and the AuNPs easily peel off the surface of the PDMS films, whereas the latter method enables the in-situ formation of AuNPs in a PDMS matrix without a reducing agent and premade AuNPs, because the curing agent in Sylgard 184 kit acts as reducing agent. Therefore, herein, we prepared Au-PDMS films via the in-situ synthesis method.

In cured PDMS, the residual silicon hydride (Si-H) groups of the curing agent was acted as the direct reducing agent to reduce Au ions ($AuCl_4^-$). Water molecule oxidizes Si-H and electrons give out Au ions to reduce itself [19]. When pre-cured PDMS was used to prepare Au-PDMS films, the population of AuNPs in the films depended on the incubation time [17]. Namely, Au ions slowly diffused into the inside and reacted with residual Si-H groups, resulting in the formation of AuNPs. However, in this work, uncured-PDMS was mixed with Au salts, and thus AuNPs get embedded homogeneously in the PDMS without aggregation. When the mass ratio of elastomer to curing agent increased, the AuNPs could aggregate on the surface or inner matrix due to the fast reduction of the Au salts [17].

UV-vis absorption spectroscopy was used to monitor the plasmon absorption of AuNPs produced in Au-PDMS films. Pure PDMS films show no absorbance peak in the visible region, whereas the Au-PDMS films have an absorbance peak centered at ca. 530 nm (Fig. 3(a)). This absorption band is due to the surface plasmon excitation of the AuNPs and confirms the AuNPs formation in the Au-PDMS films. It is consistent with the TEM analysis of the AuNPs formation (Fig. 2(b)). The absorption intensity increased with the initial contents of Au salts, indicating the formation and increasing population of AuNPs in the Au-PDMS films. As the refractive index near the NPs surface increases, the extinction spectrum of AuNPs shifts to a longer wavelength [25]. Since the refractive index of PDMS (n=1.42) is slightly larger than that of water (n=1.33), the absorbance peak of the AuNPs was slightly redshifted to ca. 530 nm, compared to that of AuNPs in water (ca. 520 nm). As the AuNPs' content in the Au-PDMS films increased, the absorbance intensity in the infrared region generally increased (Fig. 3(b)). If

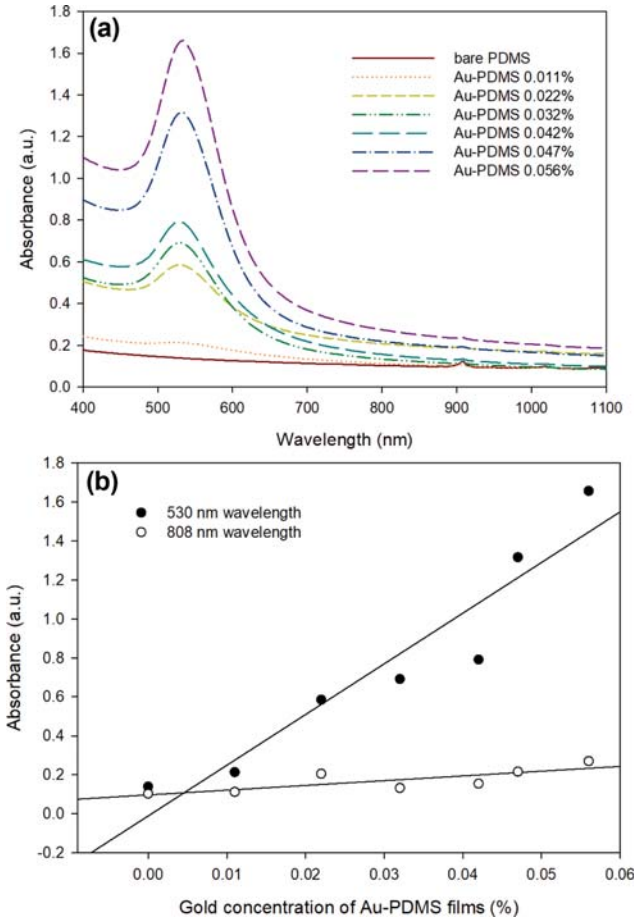

Fig. 3. (a) UV-vis spectrum of Au-PDMS films, and (b) absorbance change at 530 and 808 nm wavelength with AuNP concentration in Au-PDMS matrix.

the AuNPs aggregated with neighboring AuNPs in the Au-PDMS films, an additional new peak would appear as a second plasmon band in the infrared region due to the coupling between the surface plasmon of neighboring AuNPs [26]. However, as shown in Fig. 3(a), no characteristic peaks in the infrared region were found. In addition, the characteristic peak at 530 nm for spherical AuNPs was not shifted as the AuNPs' content in the films increased. This result indicates that the AuNPs in the films did not form aggregates and maintained their primary size.

Some fillers, such as carbon nanotube and carbon black, in a stretchable substrate have shown an enhanced absorbance in the NIR region [19,27]. Therefore, the increased absorbance of AuNPs in the NIR region could be helpful to enhance the photothermal performance of Au-PDMS films under NIR irradiation. The enhanced photothermal performance can be easily measured using the maximum temperature of the Au-PDMS films under NIR irradiation. The change in elevation temperature on the surface of the Au-PDMS films via photothermal heating was measured by an IR camera. 808 nm is commonly used in NIR-induced photothermal therapy [7] because NIR light can provide a deeper radiation penetration through tissue and polymer films. Thus, AuNPs in the polymer matrix readily transform the photon energy absorbed from

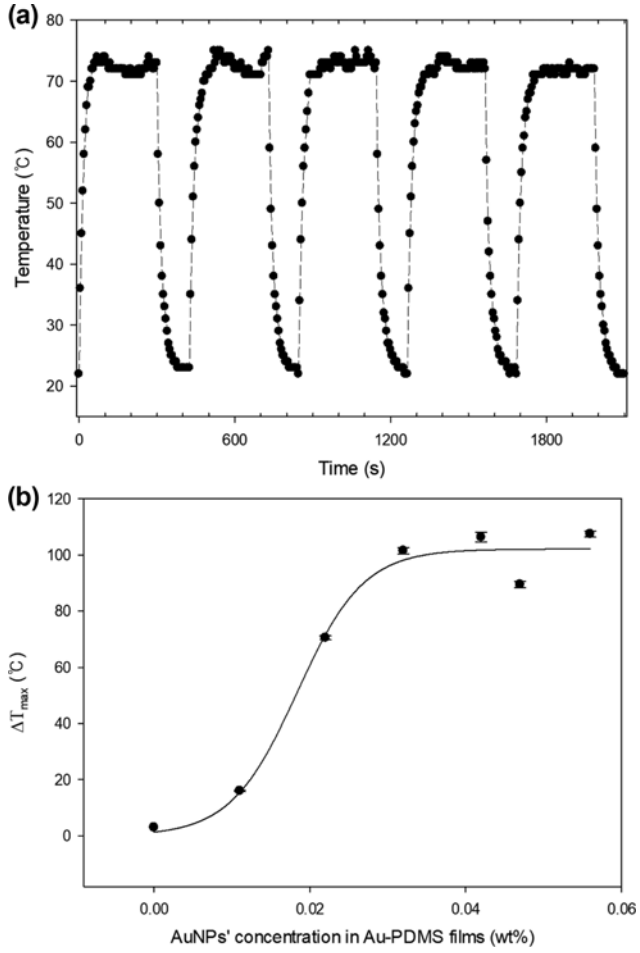

Fig. 4. (a) Temperature change of 0.022% Au-PDMS film with NIR irradiation on/off, and (b) maximum temperature change of Au-PDMS films at 0% strain.

NIR light into heat energy. The surface temperature of 0.022% Au-PDMS films rapidly increased and reached equilibrium within 1 min, and quickly cooled after the laser was turned off (Fig. 4(a)). When the PDMS film was heated on the hot-plate, its surface temperature was slowly elevated at on-step and slowly cooled at off-step. While the heating of PDMS required a large amount of energy, the localized heating of the AuNPs via the photothermal effect required very low light energy. Therefore, the cyclic heating-cooling of Au-PDMS films was shown to be a fast and repeatable process. During five cycles of the heating-cooling, their photothermal performance was maintained, indicating that Au-PDMS has good thermal stability.

As shown in Fig. 4(b), the surface temperature change (ΔT) of Au-PDMS films increased with increasing AuNPs' contents in the films. While pure-PDMS showed a slight temperature change (2 °C), the Au-PDMS films with AuNP content >0.03% revealed a large temperature change (ca. 100 °C) due to the high loading of the AuNPs in the films and enhanced absorbance in the NIR region. While energy dissipation from individual AuNPs under NIR irradiation is modest, the simultaneous resonant irradiation of an AuNP ensemble produces macroscopic bulk heating [22]. For low content of AuNPs, the photothermal behavior was considered as the summation of the response of individual AuNPs in the matrix. For high content of AuNPs, the temperature increase of each NP results from the superposition of the heating effect via the photothermal feature due to its own light absorption and the heat fluxes that diffuse from its neighboring NPs [6]. Namely, the large temperature change was induced by the thermal superposition and plasmonic coupling among NPs. Therefore, these two effects were revealed at high content of AuNPs in Au-PDMS films. Above 0.042% AuNP content, the temperature change was less compared to ΔT of 0.032% AuNPs. This may be due to the limitation of the heat capacity and fast thermal effusivity (ε).

The specific heat capacity (C_p), thermal conductivity (k), and density (ρ) for PDMS are 1,460 kJ/(kgK), 0.16 W/(mK), and 970 kg/m^3, respectively. Those of Au are 0.128 kJ/(kgK), 317.9 W/(mK), and 19,320 kg/m^3, respectively [22]. The specific heat capacity of the Au-PDMS films was assumed to be that of pure-PDMS, as there was a low-mass fraction of AuNPs in the films. Thus, the specific heat capacity of Au-PDMS films dominated with that of PDMS. The thermal energy accumulated between the NPs via photothermal effect is readily dissipated to the surroundings, i.e., PDMS matrix. Even though PDMS has a large heat capacity, the heat energy accumulated at the PDMS can be released to reach thermal equilibrium between the surface of the PDMS and external air. Therefore, the maximum elevation of temperature changed less after 0.042% AuNPs. In addition, a material's thermal effusivity [$\varepsilon=(k\rho C_p)^{1/2}$] is a measure of its ability to exchange thermal energy with its surroundings. The thermal effusivity and conductivity of PDMS and AuNPs are 476 W$^{1/2}$kJ$^{1/2}$/(m^{2}K) and 0.16 W/(mK), and 886 W$^{1/2}$kJ$^{1/2}$/(m^{2}K) and 317.9 W/(mK), respectively. The effusivity of the AuNPs was two-times larger than that of PDMS. Therefore, local heat induced by the AuNPs is readily transferred to the PDMS and its accumulated energy is also released outward via radiation and conduction [22].

When NIR was irradiated on the AuNPs, the localized surface plasmon was excited in a near field localized at the particle surface. In addition, the near field on the AuNPs interacts with that on a neighboring one in close proximity, coupling the plasmon oscillation together [23]. As the plasmon coupling strength is a function of the interparticle distance (d^{-3}), the interparticle electromagnetic coupling may decay with the mechanical stretching of the Au-PDMS films. As shown in Fig. 5(a), the decrease in temperature elevation with strain reflects the reduced plasmon coupling strength. 100% of strain doubles the length of the Au-PDMS films. In the case of 100% strain for 0.032% Au-PDMS film, the surface temperature decreased to 105 °C compared to 0% strain (118 °C). As the strain increased along the *x*-axis, the surface temperature gradually decreased. This feature was also found in the case of 0.022% Au-PDMS films (Fig. 5(b)). Note that the interparticle distance between the AuNPs in Au-PDMS films widened with increasing the strain, and the density of the AuNPs capable of photothermal heating per unit area decreased. The density (μg/mm^2) of AuNPs in the films was calculated based on the mass % in the films; the 0.022% and 0.032% Au-PDMS films showed 0.233 and 0.339 μg/mm^2, respectively. The increase in strain (*x*-axis expansion) caused a decrease in the number of AuNPs per unit area; thus, photother-

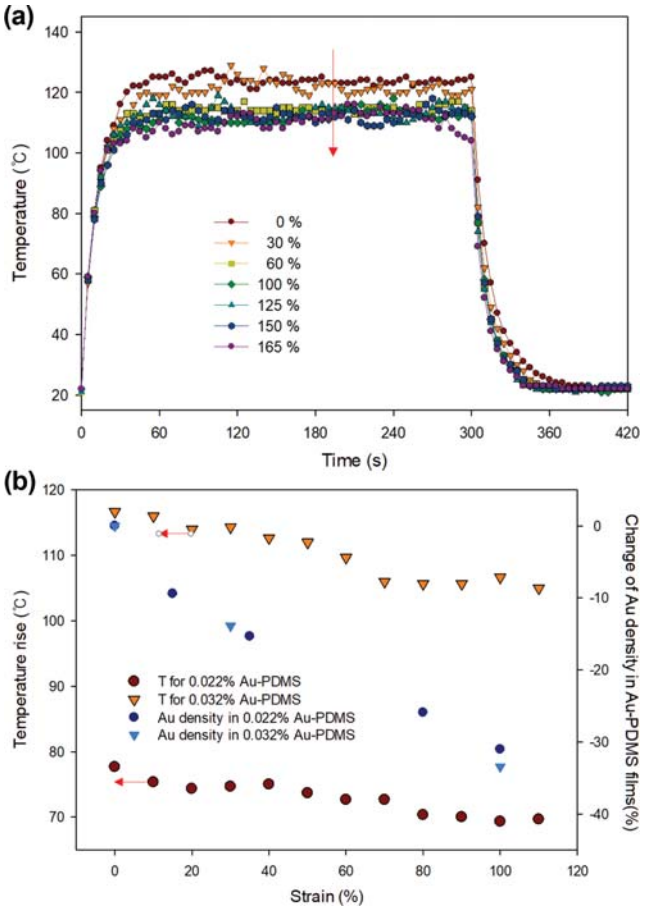

Fig. 5. (a) Temperature profiles of 0.032% Au-PDMS with change of strain for film stretching, and (b) change of AuNPs' density per unit area in 0.022% and 0.032% Au-PDMS films.

mal performance was reduced in the strained film. Hence, the decreased coupling effect and the widened area of films resulted in a decrease of the heat source and an increase of the heat sink (dissipation). Meanwhile, shrinking of the films along the *y*-axis for continuous stretching along the *x*-axis induced the nonintentional decreased in interparticle spacing. However, the increase of the interparticle distance along the *x*-axis is more dominant than the decrease of that along the *y*-axis. Therefore, the films' temperature decreased with strain along the *x*-axis.

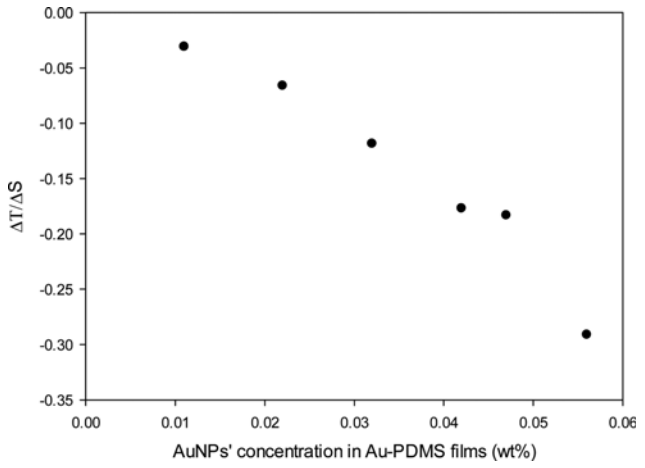

Fig. 6. Deviation of temperature (ΔT) to strain (ΔS) of Au-PDMS films with increasing AuNP concentration.

The deviation of the temperature to strain (ΔT/ΔS) is represented in Fig. 6. The photothermal performance for heat generation is much weaker for high content of AuNPs in Au-PDMS films, as heat dissipation occurs easily through the expanded film surface with increasing strain. For high content of AuNPs, the deviation is larger than that for low content of AuNPs. From the above results, the surface temperature of the plasmonic patch comprising metallic NPs embedded on PDMS could be adjusted by changing the mechanical stretching (relaxation for *x*-axis or contraction for *y*-axis and *z*-axis). Therefore, under NIR irradiation, Au-PDMS has a potential application as a heating bandage for muscular pain or wound treatment with good photothermal performance that can be adjusted by the user.

CONCLUSIONS

AuNPs embedded on a PDMS matrix were successfully prepared by the in-situ synthesis method without a reducing agent. The curing agent in the PDMS kit acted as an effective reductant to form the AuNPs (24 nm) in the PDMS matrix. The content of AuNPs in the Au-PDMS films was easily adjusted with the initial concentration of Au salts, and the formation of the AuNPs was confirmed by TEM and UV-vis analysis. The photothermal performance of the Au-PDMS films was evaluated with NIR irradiation. The surface temperature of the films increased to a maximum of ca. 120 °C, induced by the superposition of its own light absorption of individual AuNP and heat fluxes from its neighboring NPs. The effusivity of AuNPs is larger than that of PDMS; thus the photothermal local heating readily transferred into PDMS and its accumulated energy was released outward via radiation and conduction. This feature results in a fast heating and cooling performance in the cyclic test. In the mechanical stretching test, the surface temperature of the Au-PDMS films gradually decreased as the strain increased along the *x*-axis. This may be due to the extended interparticle distance between AuNPs in the strained Au-PDMS and the decreasing density of the AuNPs per unit area.

ACKNOWLEDGEMENTS

This work was conducted with a research fund of the National Research Foundation of Korea (NRF-2017R1A2B4001829). Hwang gratefully acknowledges support from Canada Research Chairs program.

REFERENCES

1. H. N. Umh and Y. Kim, *Korean J. Chem. Eng.*, **30**, 482 (2013).
2. C. Fasciani, C. J. B. Alejo, M. Grenier, J. C. Netto-Ferreira and J. C. Scaiano, *Org. Lett.*, **13**, 204 (2011).
3. H. Liao, C. L. Bebl and J. H. Hafner, *Nanomed.*, **1**, 201 (2006).
4. X. Zhang, X. Ke, A. Du and H. Zhu, *Sci. Rep.*, **4**, 3805 (2014).
5. Q. Gan, F. J. Bartoli and Z. H. Kafafi, *Adv. Mater.*, **25**, 2385 (2013).

6. V. Siahpoush, S. Ahmadi-kandjani and A. Nikniazi, *Opt. Commun.*, **420**, 52 (2018).
7. Y. Hu, X. Liu, Z. Cai, H. Zhang, H. Gao, W. He, P. Wu, C. Cai, J.-J. Zhu and Z. Yan, *Chem. Mater.*, **31**, 471 (2019).
8. P. Wu, D. Deng, J. Gao and C. Cai, *ACS Appl. Mater. Interfaces*, **8**, 10243 (2016).
9. F. Wang, C. Li, H. Chen, R. Jiang, L-D. Sun, Q. Li, J. Wang, J. C. Yu and C.-H. Yan, *J. Am. Chem. Soc.*, **135**, 5588 (2013).
10. C. Leduc, S. Si, J. Gautier, M. Soto-Ribeiro, B. Wehrle-Haller, A. Gautreau, G. Giannone, L. Cognet and B. Lounis, *Nano Lett.*, **13**, 1489 (2013).
11. S. Toroghi and P. G. Kik, *Phys. Rev. B*, **90**, 205414 (2014).
12. D. Qiu, L. Gu, X.-L. Sun, D.-H. Ren, Z.-G. Gu and Z. Li, *RSC Adv.*, **4**, 61313 (2014).
13. M. Hu, J. Chen, Z.-Y. Li, L. Au, G. V. Hartland, X. Li, M. Marquez and Y. Xia, *Chem. Soc. Rev.*, **35**, 1084 (2006).
14. J. Ge, L. Sun, F.-R. Zhang, Y. Zhang, L.-A. Shi, H.-Y. Zhao, H.-W. Zhu, H.-L. Jiang and S.-H. Yu, *Adv. Mater.*, **28**, 722 (2016).
15. H. SadAbadi, S. Badilescu, M. Packirisamy and R. Wüthrich, *J. Biomed. Nanotechnol.*, **8**, 1 (2012).
16. J. Luan, J. J. Morrissey, Z. Wang, H. G. Derami, K.-K. Liu, S. Cao, Q. Jiang, C. Wang, E. D. Kharasch, R. R. Naik and S. Singamaneni, *Light Sci. Appl.*, **7**, 29 (2018).
17. Q. Zhang, J.-J. Xu, Y. Liu and H.-Y. Chen, *Lab Chip*, **8**, 352 (2008).
18. U. Cataldi, R. Caputo, Y. Kurylyak, G. Klein, M. Chekini, C. Umeton and T. Bürgi, *J. Mater. Chem. C*, **2**, 7927 (2014).
19. R. Gupta, H. K. Nagamanasa, R. Ganapathy and G. U. Kulkarni, *Bull. Mater. Sci.*, **38**, 817 (2015).
20. A. Goyal, A. Kumar, P. K. Patra, S. Mahendra, S. Tabatabaei, P. J. J. Alvarez, G. John and P. M. Ajayan, *Macromol. Rapid Commun.*, **30**, 1116 (2009).
21. A. M. Alkilany and C. J. Murphy, *J. Nanopart. Res.*, **12**, 2313 (2010).
22. J. R. Dunklin, G. T. Forcherio, K. R. Berry Jr. and D. K. Roper, *J. Phys. Chem. C*, **118**, 7523 (2014).
23. E. Bedogni, S. Kaneko, S. Fujii and M. Kiguchi, *Jap. J. App. Phys.*, **56**, 035201 (2017).
24. M.-C. Lim, K. Park, S.-H. Kim, G. Ok and S.-W. Choi, *Colloids Surf., A*, **529**, 916 (2017).
25. C. Novo, A. M. Funston, I. Pastoriza-Santos, L. M. Liz-Marzán and P. Mulvaney, *J. Phys. Chem. C*, **112**, 3 (2008).
26. M. Doyen, J. Goole, K. Bartik and G. Bruylants, *J. Colloid Interface Sci.*, **464**, 160 (2016).
27. E. Miyako, C. Hosokawa, M. Kojima, M. Yudasaka, R. Funahashi, I. Oishi, Y. Hagihara, M. Shichiri, M. Takashima, K. Nishio and Y. Yoshida, *Angew. Chem. Int. Ed.*, **50**, 12266 (2011).